Evolution of structure and lithium dynamics in $LiNi_{0.8}Mn_{0.1}Co_{0.1}O_2$ (NMC811) cathodes during electrochemical cycling

Katharina Märker,[1,2] Philip J. Reeves,[1] Chao Xu,[1,2] Kent J. Griffith,[1,3] Clare P. Grey*,[1,2]

[1] Department of Chemistry, University of Cambridge, Lensfield Road, Cambridge CB2 1EW, United Kingdom.

[2] The Faraday Institution, Quad One, Harwell Science and Innovation Campus, Didcot, United Kingdom.

[3] Present address: Department of Materials Science and Engineering, Northwestern University, Evanston, IL, USA.

ABSTRACT: The nickel-rich layered oxide $LiNi_{0.8}Mn_{0.1}Co_{0.1}O_2$ (NMC811) is a promising future cathode material for lithium-ion batteries in electric vehicles due to its high specific energy density. However, it exhibits fast voltage and capacity fading. In this article, we combine electrochemistry, *operando* synchrotron X-ray diffraction (XRD), and *ex situ* solid-state NMR spectroscopy to provide new insights into the structural changes and lithium dynamics of NMC811 during electrochemical charge and discharge, which are essential for a better understanding of its fast degradation. The evolution of the interlayer spacing is tracked by XRD, showing that it gradually increases upon delithiation before collapsing at high state-of-charge (SOC). Importantly, no two-phase O3→O1 transition is observed at high SOC, demonstrating that this cannot be a major cause of degradation. A strong increase of Li dynamics accompanies the increase of the interlayer spacing, which is shown by ^{7}Li NMR and electrochemical characterization. At high SOC, Li mobility drops considerably, and Li/vacancy ordering can be observed by NMR. A detailed analysis of ^{7}Li NMR spectra at different SOC is provided, demonstrating how Li NMR can be used to extract information on the dynamics of such challenging paramagnetic samples with several hundred different local Li environments. The insights on the evolution of structure and dynamics of NMC811 will further the understanding of its cycling behavior and contribute to the efforts of mitigating its performance fade.

INTRODUCTION

Improved rechargeable batteries are required to enable the shift of the automotive industry from internal combustion engines to electric motors. Lithium-ion batteries (LIBs) are considered as the most promising candidates to enable electromobility with a reasonable driving range at an affordable cost, largely due to their high energy density and long lifetimes. The first-generation cathode material in commercial LIBs, the layered material $LiCoO_2$, has a limited practical capacity (~155 mAh g^{-1}) and research has, therefore, been devoted to develop cheaper alternatives with higher energy densities and higher rates. One promising approach is to replace part of the cobalt by other transition metals (TMs) such as nickel and manganese. This yields isostructural materials, $LiNi_xMn_yCo_zO_2$, which are usually referred to as NMC*XYZ*,[1] with *X*, *Y* and *Z* indicating the Ni, Mn and Co molar ratios. Such NMC materials have already been commercialized for use in LIBs in a variety of ratios (NMC111, NMC532, NMC622). However, a great interest still lies in NMC materials with even higher nickel content as they can provide higher specific capacity within the same voltage window and further decrease dependence on scarce, geographically-concentrated, and expensive cobalt.[2,3]

NMC811 ($LiNi_{0.8}Mn_{0.1}Co_{0.1}O_2$) is a Ni-rich NMC composition that is currently attracting considerable attention as a future cathode material. It can deliver a high specific capacity of ~200 mAh g^{-1} with a moderately high average discharge potential of ~3.8 V vs Li^+/Li, resulting in a substantial increase of ~25% in energy density compared to $LiCoO_2$ (based on the cathode material only).[3] NMC811 adopts the α–$NaFeO_2$ layered oxide structure, which is characterized by a close-packed oxygen lattice and alternating layers of lithium and TM ions in octahedral coordination environments.[4]

Severe challenges still need to be overcome in order to achieve successful commercialization of NMC811 cathodes, most importantly their considerably faster voltage and capacity fading as compared to NMC materials with lower Ni content.[2,5] Moreover, Ni-rich NMCs exhibit poorer chemical stability under ambient conditions and poorer thermal stability.[2,6,7] It is still not fully understood what causes the fast performance fading, although it is widely acknowledged that it arises at least in part from processes that occur, or are initiated, at high state-of-charge (SOC), as performance fading is much more severe when cells are charged beyond ~4.2 V vs Li^+/Li.[5]

Charging to high voltages is accompanied by a clear redox process at ~4.2 V in the differential capacity profile that is not present for NMC materials with lower Ni content.[2,5] In the structurally-related $LiNiO_2$, a similar redox peak is observed in the differential capacity profile at the top of charge and is assigned to a two-phase O3→O1 transition caused by shearing of the TM-O layers.[8,9] The O3/O1 classification was introduced by Delmas et al.,[10] the "O" signifying that lithium is in an octahedral coordination environment, and "3" and "1" indicating that there are three and one NiO_2 sheets in the crystallographic repeat unit, respectively.[10] In the context of $LiNiO_2$ and Ni-rich

NMCs, the O3 and O1 phases are often referred to as H2 and H3, following the naming used in an *in situ* X-ray diffraction (XRD) study of $LiNiO_2$, where they correspond to the second and third hexagonal phases found during charge.[8] The O3→O1 transition in $LiNiO_2$ and the associated strain developed in the lattice lead to particle cracking and strongly impair its cycling stability.[8,9]

It has been hypothesized that the degradation processes that occur in $LiNiO_2$ cells could also be the cause of capacity fade in Ni-rich NMCs. Moreover, observed release of lattice oxygen at high voltages has also been associated with the occurrence of a two-phase O3→O1 transition.[5] This is, however, inconsistent with prior laboratory *in situ* XRD experiments that do not show a two-phase region at high SOC of NMC811.[4,11] Nevertheless, the XRD experiments demonstrate pronounced changes of the *c* lattice parameter during electrochemical cycling which corresponds to a change of the interlayer spacing: It first increases during charge before it collapses drastically above ~4.2 V, meaning that this collapse is correlated to the occurrence of the redox peak in the differential capacity profile.[4,11] Despite these structural changes, no particle cracks were observed by scanning electron microscopy of cycled cathodes,[4,11] suggesting that they may not be the main reason for cell failure. Other processes may therefore be more crucial, including parasitic reactions arising from interactions between the electrolyte and the highly reactive delithiated cathode surface.

Apart from the structural changes upon electrochemical cycling of NMC811 cathodes, it is also essential to understand the diffusivity of Li ions, which plays an important role in the kinetics of battery cycling and in battery degradation.[12] Fast Li diffusion can enable fast charging of batteries, which is of great importance for application in electric vehicles. Sluggish Li diffusion, on the other hand, causes overpotentials to build up, leading to reduced utilization of the cathode material and hence reduced capacity.[12] This effect becomes more severe at faster charge/discharge rates and can cause heating of the cell which accelerates degradation. In layered NMC materials, the transport of Li ions is governed by Li hopping between two neighboring octahedral sites through an adjacent tetrahedral site.[12,13] This tetrahedral site shares faces with four octahedral sites, three in the Li layer and one in the TM layer. Generally, the activation barrier for a Li ion hopping from an occupied site into an adjacent vacant Li site is lowered when the second adjacent Li site is vacant too (a "divacancy hop"), and/or when the adjacent TM ion is in a low oxidation state.[13–15] Both situations lead to lower electrostatic repulsion along the hopping trajectory. Li hopping and the migration barriers are therefore very sensitive to the local structure. Noh et al. used the galvanostatic intermittent titration technique (GITT) to measure Li diffusion coefficients in a series of NMC materials and observed increasing Li diffusivity with increasing Ni content.[2] The chemical diffusion coefficient in NMC811 ranges between 10^{-12} to 10^{-13} m^2 s^{-1} in their measurements and varies depending on the SOC.[2]

In the present study, we provide new insights into the structural and dynamic processes that occur during charge and discharge of NMC811 cathodes. We present *operando* synchrotron XRD data which confirms that there is no two-phase transition at the top of charge, during the electrochemical cycling of the material. Moreover, we present a series of *ex situ* ^{7}Li solid-state nuclear magnetic resonance (NMR) spectra of NMC811 cathodes, recorded at different SOC. This data shows that substantial Li ion mobility persists until ~70% SOC. Moreover, Li diffusion rates are not uniform over the whole sample and a small fraction of mobile Li ions still remains at high SOC. These findings are supported by variable temperature (VT) NMR experiments and electrochemical data obtained with GITT. These insights further the understanding of changes in structure and dynamics during charge and discharge of Ni-rich NMC materials and will help to optimize their use in LIBs.

MATERIALS AND METHODS

Materials. Printed NMC811 electrodes were fabricated in Argonne National Laboratory (A-C020, made by CAMP facility) with the following materials: 90 wt% NMC811 (Targray), 5 wt% conductive carbon (Timcal C45) and 5 wt% PVDF binder (Solvay 5130). The electrode sheet was calendared to a thickness of ~52 μm (including 20 μm Al foil) and a porosity of ~36.3%. The areal loading of the NMC811 active material is 8.34 mg cm^{-2}. Circular electrodes with a diameter of ½ inch (12.7 mm) were punched out and dried at 120°C under dynamic vacuum prior to cell assembly. The electrolyte used in the present study is LP30 (1.0 M $LiPF_6$, ethylene carbonate (EC):dimethyl carbonate (DMC) 1:1 v/v, battery grade, Sigma Aldrich). Li metal (99.95%) disks were purchased from LTS Research Laboratories, Inc. All procedures described below (sample preparation, coin cell assembly and disassembly, packing of NMR rotors) were performed in an argon-filled glove box with water and oxygen levels below 10 ppm.

Electrochemical characterization. All electrochemical tests in this work were performed on NMC/Li half-cells in 2032 coin-cell configuration (Cambridge Energy Solutions). One ½ inch cathode, one 5/8 inch glass fiber separator (GF/B, Whatman) soaked with 150 μL LP30 electrolyte, and one Li metal disk were stacked and assembled into the coin cell.

Galvanostatic cycling tests on NMC/Li half-cells were conducted at room temperature (20 ± 2 °C) on a VMP2 potentiostat (Biologic) at a current density of 10 mA g^{-1} of NMC811 (equivalent to a rate of C/20 assuming the capacity of NMC811 is 200 mAh g^{-1}). All electrochemical potentials discussed in this work are referenced to Li^+/Li.

GITT experiments were also performed on NMC811/Li half-cells. Galvanostatic current pulses were applied with magnitudes of 10 mA g^{-1} for 30 minutes, followed by a 4 hour rest period. The diffusion coefficient of Li^+, D_s, can be calculated based on the following equation:[16,17]

$$D_s = \frac{4}{\pi}\left(\frac{IV_m}{FS}\right)^2\left(\frac{dU^0/dy}{dV/d\sqrt{t}}\right)^2, \qquad t \ll R^2/D_s \qquad [1]$$

where I is the current of the short pulses, V_m is the molar volume of NMC811, F is Faraday's constant, S is the active area of the composite electrode, U_0 is the open circuit voltage (OCV) of the NMC811 electrode at the end of each rest period, y is the SOC (i.e. y in $Li_{(1-y)}Ni_{0.8}Mn_{0.1}Co_{0.1}O_2$), V and t are the voltage and time during pulse periods, respectively, and R is the diffusion length. The molar volume V_m and active surface area S are factors difficult to obtain accurately due to the complex nature of the composite electrode, as it contains multiple active and inactive materials, various pores and voids, as well as particles of

varying size. Therefore, it is very difficult to obtain accurate absolute diffusion coefficients from GITT experiments.[17] In this work, we assume that V_m and S remain unchanged, and we investigate the relative changes in Li mobility using the following equation:[17]

$$\frac{D_s S^2}{{V_m}^2} = \frac{4}{\pi}\left(\frac{I}{F}\right)^2 \left(\frac{dU^0/dy}{dV/d\sqrt{t}}\right)^2 \qquad [2]$$

The approach for determining dU^0/dy and $dV/d\sqrt{t}$ was adopted from Verma et al.[17] Briefly, the experimentally obtained U^0 vs y profile was curve-fitted using a polynomial function, which was then differentiated to determine the values of dU^0/dy as a function of y. $dV/d\sqrt{t}$ values were obtained as the slope of the linear function of V vs $\sqrt{t}$. These linear fittings were performed in the range of 100 s < t < 1800 s to ensure a good fit.

Neutron diffraction. Constant-wavelength (1.5483 Å) neutron diffraction was performed on the SPODI[18] high-resolution diffraction beamline at the Heinz Maier-Leibnitz Zentrum (MLZ) in Garching, Germany. More than 12 g NMC811 was packed in an argon glovebox into a 13 mm diameter cylindrical sample holder of vanadium and sealed with compressed indium wire. The sample height completely spanned the neutron irradiation height of 50 mm.

***Operando* synchrotron X-ray diffraction**. *Operando* powder diffraction measurements were conducted at beamline 17BM at the Advanced Photon Source, Argonne National Laboratory. The experiments were performed at room temperature using Argonne's multi-purpose *in situ* X-ray (AMPIX) cell in transmission mode at 0.24141 Å with a 2D area detector. The AMPIX cell contains a rigid, conductive glassy carbon window to ensure uniform stack pressure and thereby homogenous electrochemical behavior in the cell.[19] The NMC811 electrodes for *operando* XRD experiments were self-standing films consisting of NMC811 powder (Targray), Super P Li carbon black (TIMCAL) and poly(tetrafluoroethylene) (Sigma, free flowing powder, 1 μm) in a mass ratio of 60:30:10. A stack of NMC811 self-standing cathode, glass fiber separator soaked with LP30 electrolyte and Li metal anode was assembled into the AMPIX cells, which were galvanostatically cycled at 57.14 mA g^{-1} of NMC811 (equivalent to a rate of C/3.5 assuming the capacity of NMC811 is 200 mAh g^{-1}).

GSAS-II software was used for sequential Rietveld refinement of NMC811 during electrochemical cycling. For the pristine NMC811 material (i.e., operando cell prior to cycling), the atomic coordinates, unit-cell parameters, background, zero offset and peak shape parameters were refined and used as the initial structure. In the sequential refinement, only the unit-cell parameters, oxygen z coordinate and Chebyshev background coefficients were allowed to vary.

NMR sample preparation. NMC811/Li half-cells were cycled galvanostatically at a rate of 10 mA g^{-1}. The cycling was stopped either after a defined time to reach a certain SOC (10%, 25%, 40%, 50%, 65%) or at a defined potential (4.2 V, 4.3 V, 4.4 V, corresponding to SOC of 75%, 82%, 85%, respectively). One cell was charged to 4.4 V and held at this potential until the measured current dropped below 1 μA, which resulted in a SOC of ≥86%. After cycling, the cathodes were extracted, washed three times with DMC (~1 mL) and dried *in vacuo* for 30 minutes. The cathode material was then scraped off the current collector and packed into a 1.3 mm magic-angle spinning (MAS) NMR rotor. The NMR samples weighed between 3.2 mg and 4.3 mg.

Solid-state NMR experiments. Solid-state NMR experiments were performed on a 4.7 T (200 MHz ^{1}H Larmor frequency) Bruker Avance III spectrometer, using a Bruker 1.3 mm double resonance probe. All spectra were acquired at a MAS frequency of 60 kHz, and ^{7}Li radiofrequency (rf) pulses were applied at ~230 kHz rf field strength. Recycle delays between 20 ms and 35 ms were employed which were quantitative for the bulk signal of NMC811 (but not for the signals of diamagnetic Li salts at ~0 ppm). ^{7}Li chemical shifts were referenced externally using Li_2CO_3 (0 ppm).

For projection MATPASS[20] spectra, 8 t_1 increments were recorded. The number of transients acquired per t_1 increment varied between 10240 and 102400 depending on the Li content (i.e. SOC) of the sample.

Variable temperature (VT) spectra were acquired using a rotor-synchronized Hahn echo sequence with a total echo length of two rotor periods (33.33 μs). 10240 transients were accumulated for each spectrum. Sample temperatures are reported based on an external calibration using the chemical shift of ^{207}Pb in $Pb(NO_3)_2$.[21]

Calculation of NMR spectra. NMR spectra were calculated using a random solution model based on previously published methods.[22,23] Li hopping was incorporated using the formula derived by Norris.[24] Details on the calculations can be found in the SI.

RESULTS

Electrochemistry. Figure 1a shows the voltage profile of a NMC811/Li half-cell during the first cycle between 4.4 V and 3.0 V. NMC811 exhibits a high full-charge capacity of 240 mAh g^{-1} and discharge capacity of 200 mAh g^{-1}, placing it among the highest capacity cathode materials for LIBs. The voltage curve is relatively featureless compared to that of $LiNiO_2$, where several plateau regions are associated with distinct first-order (two-phase) structural phase transformations.[8,9] To visualize the remaining details in the voltage profile, incremental capacity analysis was carried out and the resulting dQ/dV vs voltage plot is presented in Figure 1b. Three regions, which contribute the majority of the capacity, are highlighted in Figure 1 as regions I, II, and III. Very limited capacity (<20 mAh g^{-1}) is achieved in region IV. The maxima of the three peaks in regions I, II and III during charge are found at 3.68, 4.00, and 4.21 V vs Li^+/Li, respectively, which is consistent with previous reports.[2,4,11] Moreover, similar features are also observed in $LiNiO_2$ cell chemistry, in which these peaks are coupled with distinct first-order phase transitions.[8,9,12,25] To verify whether these phase transitions also occur in NMC811 materials, we performed *operando* synchrotron XRD experiments which reveal the structural changes in NMC811 during cycling.

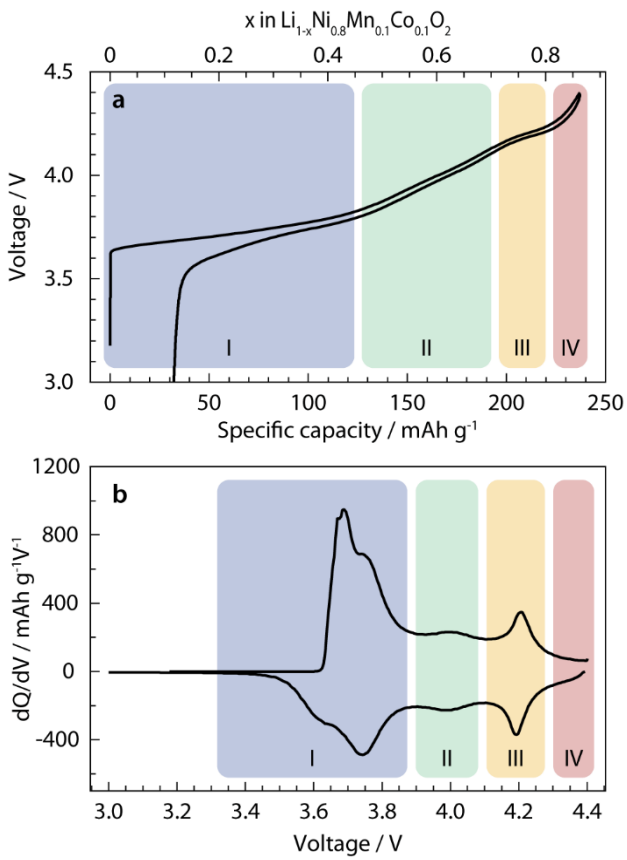

Figure 1. First charge and discharge voltage curve of a NMC/Li half-cell (a) and the corresponding differential capacity (dQ/dV) plot (b).

Neutron diffraction. A high-resolution neutron diffraction pattern of NMC811 powder was collected at room temperature before manufacturing electrodes. No evidence of secondary phases, superstructure peaks, or distorted line shapes was observed (see Figure S10). Thus, the material used here for NMC811 electrodes is phase pure and free of significant stacking disorder or strain.

***Operando* synchrotron X-ray diffraction.** *Operando* XRD data was recorded using Argonne's multipurpose *in situ* X-ray (AMPIX) cells[19] and very hard synchrotron X-ray radiation (51 keV). The rigid and electrically-conducting glassy carbon X-ray window used in these cells ensures homogenous electrochemical cycling of the battery materials without sacrificing transparency. Most importantly, the use of AMPIX cells combined with high energy synchrotron radiation and an area detector enabled us to record 'instantaneous' snapshots of the material during electrochemical cycling, such that we are averaging over less than 0.0005 Li transferred (per formula unit of $LiNi_{0.8}Mn_{0.1}Co_{0.1}O_2$) for each XRD pattern. This ensures that we do not miss phase transitions that may occur over very short time periods and therefore enables us to detect all possible structural changes which are observable by XRD.

The *operando* XRD measurements were carried out on a NMC811/Li half-cell during its first electrochemical cycle between 4.4 V and 3.0 V. The diffraction patterns obtained along with the voltage profile of the electrochemical cell are shown in Figure 2a. Additional data acquired on cells charged to an upper cutoff voltage of 4.2 V and 4.8 V, respectively, are presented in Figure S6.

As expected, the crystal structure of the NMC811 material can be indexed in the $R\bar{3}m$ space group. A joint refinement of the X-ray pattern before cycling and neutron diffraction data of the pristine material was performed as well and can be found in Table S1. Based on this refinement, the percentage of Ni^{2+} in the Li layer is less than 1% in the NMC811 material used in this work.

At the very beginning of charge, a two-phase coexistence is observed between the pristine material and a partially delithiated phase, the latter continuing to lose more lithium as the concentration of the pristine phase decreases (Figure S8), indicating a non-equilibrium process and resembling the behavior reported by Li et al.[4] The process is irreversible and no two-phase behavior is seen on discharge (Figure S8b). A similar phenomenon was seen for $LiNi_{0.8}Co_{0.15}Al_{0.05}O_2$ (NCA), where this was ascribed to the effects of a surface layer containing Li_2CO_3.[26] This insulating coating impedes the transport of Li ions out of the NCA phase, creating an apparent two phase reaction, with particles with no or a thinner carbonate coating reacting before those with thicker coatings. As a consequence, Li_2CO_3 is at least partially removed on charging.

Beyond the initial non-equilibrium "two-phase" behavior, NMC811 undergoes a solid-solution mechanism during charge and discharge with no new phases appearing. This is in contrast to the complex phase transitions which occur during the delithiation and lithiation of $LiNiO_2$. Specifically, the O3→O'3 (also known as the H1→M) transition during the cycling of $LiNiO_2$ results in a peak splitting of the (101) reflection due to the formation of a new monoclinic phase and the O3→O1 (also known as H2→H3) transition, which happens at high SOC of $Li_{1-x}NiO_2$, gives rise to another (003) signal at higher 2θ angles.[8,9,12,25] However, neither of these phenomena are observed in our *operando* experiment as highlighted in Figure S7, which shows the enlarged regions of the (003) and (101) reflections on the first charge. According to these results, we note that no distinct two-phase transitions occur during the electrochemical delithiation and lithiation of NMC811.

Figure 2b shows the evolution of the *a* and *c* lattice parameters as well as the unit cell volume during electrochemical delithiation of NMC811. The trends are analogous to what has been observed in previous studies[4,11] and are typical for the delithiation behavior of layered lithium TM oxides. The *a* lattice parameter decreases upon charging to 4.4 V by maximum 2.1% (from 2.87 Å to 2.81 Å). The *c* lattice parameter shows a non-monotonic behavior: initially, it increases until a potential of ~4.1 V is reached (from 14.2 Å to 14.5 Å, $\Delta c = 2.1\%$) which means that the interlayer spacing increases. Above ~4.1 V (~70% SOC), it rapidly collapses, reaching values smaller than in the fully lithiated state when the potential exceeds 4.2 V. The unit cell volume shrinks continuously upon delithiation. While the initial lattice contraction is rather moderate and is dominated by the *a* lattice parameter up to ~4.1 V, it then shrinks more rapidly, reflecting the collapse of the *c* lattice parameter. All these trends in lattice response to lithium composition are reversible on the first discharge (see Figure S6). A closer look at the evolution of the interlayer spacing reveals that the Li and TM layers behave differently (Figure S9): As the *c* lattice parameter increases, the Li layer expands while the thickness of

the TM layer decreases. The latter is caused by the decrease in the ionic radius of the nickel ions and the increased covalency of the Ni–O bonds with increasing charge of the Ni ions. The subsequent decrease of the *c* lattice parameter is initially caused by further contraction of the TM layer, which is then followed by the collapse of the Li layer from ~75% SOC.

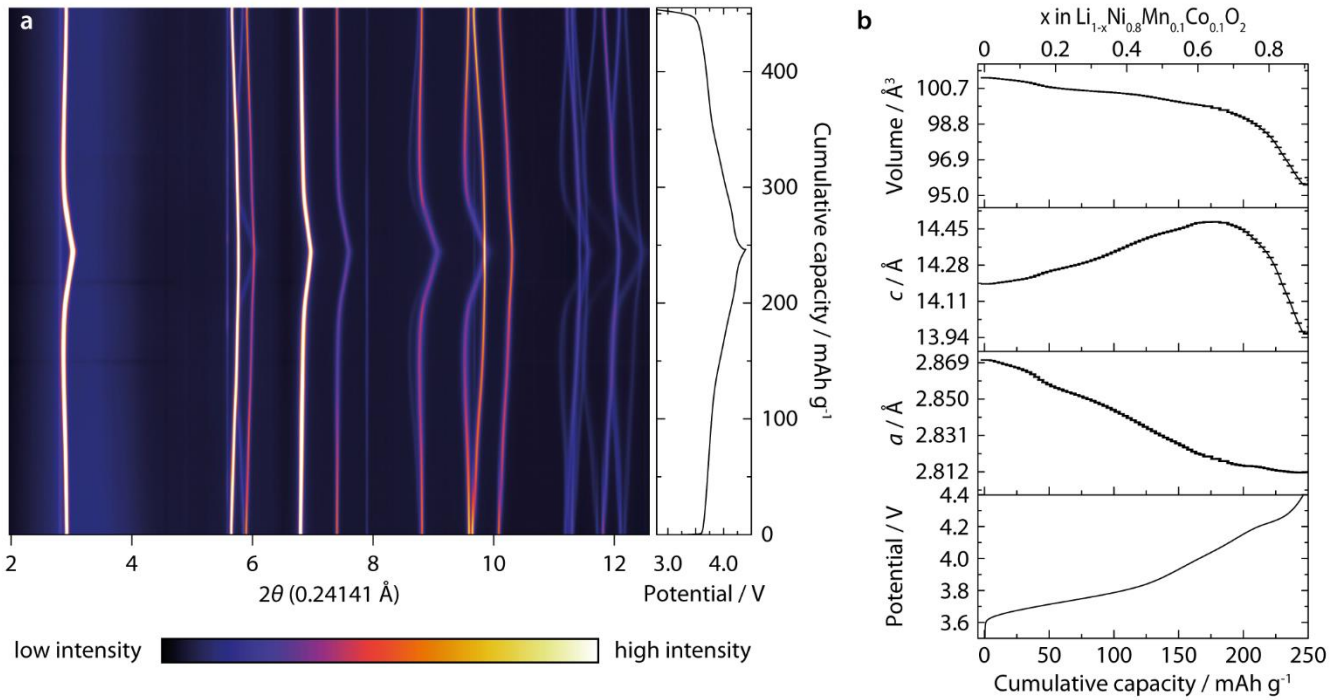

Figure 2. (a) *Operando* synchrotron XRD patterns obtained on a NMC811/Li half-cell, using an AMPIX cell[19] and very hard synchrotron X-ray radiation. (b) Evolution of the unit cell volume and *a* and *c* lattice parameters of NMC811 during the first charge to 4.4 V. The parameters were refined from the diffraction patterns in (a).

***Ex situ* ^{7}Li solid-state NMR.** While X-ray diffraction provides information regarding the evolution of long-range order and unit cell parameters, it is less sensitive to Li ions and their local structure and dynamics. For this purpose, solid-state NMR is a very powerful technique as it is extremely sensitive to the local Li environment.

The great value of lithium NMR for studying LIB cathode materials stems from the sensitivity of the lithium chemical shift to the presence of surrounding paramagnetic TM ions.[27] While lithium in a diamagnetic environment resonates close to 0 ppm, hyperfine interactions with paramagnetic ions can induce shifts of more than 100 ppm. The dominating interaction mechanism is the Fermi contact interaction which describes the transfer of unpaired electron spin density from the TM unpaired electron spins to the 2*s* orbital of lithium via the bridging oxygen atoms. The sign and magnitude of this interaction are determined by the symmetry of the TM orbital in which the unpaired spins are located and the angle of the TM–O–Li bond.[28] To a very good approximation, the hyperfine interactions with each paramagnetic neighbor can be treated separately, meaning that the induced hyperfine shifts are additive.

Typical hyperfine shifts in layered oxides have been measured experimentally[27] and can be rationalized by DFT calculations.[28] Paramagnetic TM ions in both the first and the second coordination shell of lithium affect its chemical shift through the Fermi contact interaction, and are usually referred to by the bond angle at the bridging oxygen atoms which is close to 90° and 180°, respectively. In the layered structure of NMC811, each lithium ion has in total six 90° TM neighbors and six 180° TM neighbors. As Mn^{3+}–Ni^{3+} pairs are expected to disproportionate into Mn^{4+} and Ni^{2+} in this type of material,[29] we can expect three paramagnetic species in NMC811: Ni^{2+}, Ni^{3+}, and Mn^{4+}. Their expected hyperfine shifts can be extracted from earlier experimental studies and are summarized in Table 1.[30] Co^{3+} and Ni^{4+} are diamagnetic and do not induce hyperfine shifts.

Table 1. Expected hyperfine shifts (in ppm) of ^{7}Li resonances for different paramagnetic TM ion neighbors in NMC811.[30] Shifts are given for 90° and 180° interactions.

	90°	**180°**
Ni^{2+}	–30	170
Ni^{3+}	–15	110
Mn^{4+}	250	–60

^{7}Li solid-state NMR experiments were performed on cathode materials extracted from NMC811/Li half-cells charged to different SOC, as indicated in Figure 3a. All spectra were acquired at low magnetic field (4.7 T) and fast MAS frequency (60 kHz) to reduce line broadening arising from hyperfine interactions. Figure 3b shows the ^{7}Li solid-state NMR spectra acquired *ex situ*. In general, very broad signals are observed due to the high amount of paramagnetic species in the sample and the very large number of different TM ion environments that lithium can be located in, each environment potentially leading to a different ^{7}Li chemical shift.

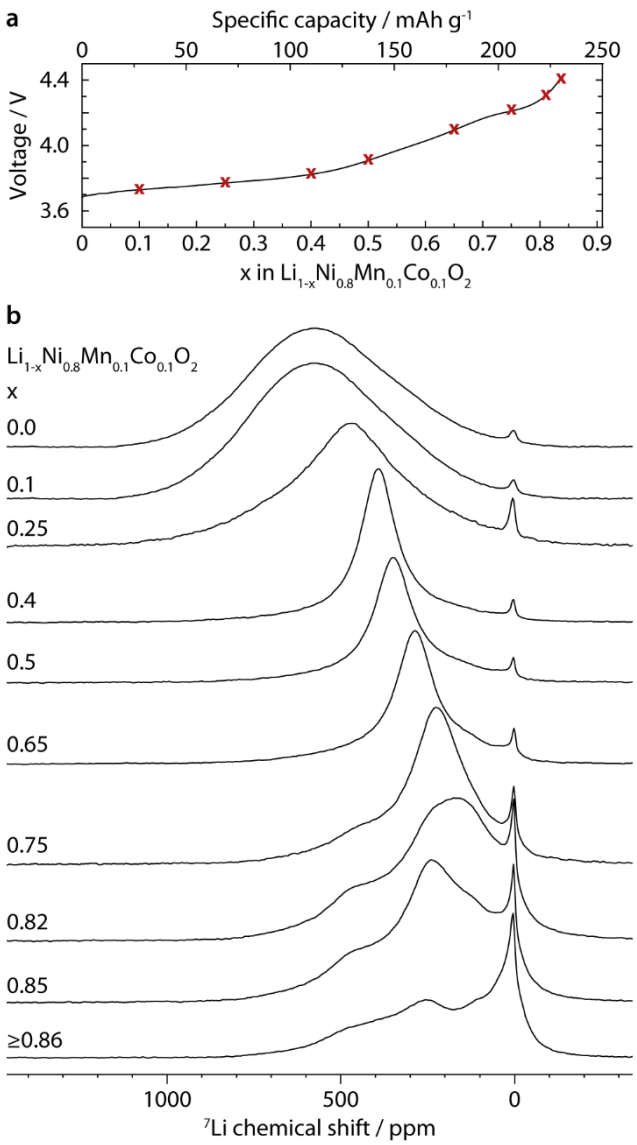

Figure 3. (a) First charge curve of a NMC811/Li half-cell with red crosses indicating where cells were stopped for *ex situ* NMR experiments. (b) ^{7}Li solid-state NMR spectra of *ex situ* NMC811 cathode sample, acquired at a magnetic field strength of 4.7 T and a MAS frequency of 60 kHz. The central slices of projection MATPASS[20] spectra are shown with an arbitrary scaling.

In the pristine material (x = 0.0), one broad signal centered at around 570 ppm is observed. This large shift of the resonance away from 0 ppm can be explained by the nearby paramagnetic Ni (80%) and Mn (10%) ions. Indeed, a hyperfine shift of 570 ppm is expected for a pure Ni^{3+} environment (six Ni^{3+}–90° and six Ni^{3+}–180° in the first and second coordination shells of the Li atom, Table 1). The substitution of Ni^{3+} ions by other TM ions creates environments with larger or smaller chemical shifts, the overlap of which leads to the very broad line shape observed experimentally. Additionally, a sharp signal at ~0 ppm is observed which occurs in all spectra in Figure 3b. This signal originates from diamagnetic lithium salts such as Li_2CO_3 on the surface of the NMC particles which can form during manufacture and storage of NMC811 electrodes.[6]

As NMC811 is delithiated, Ni^{2+} and Ni^{3+} ions are oxidized to Ni^{4+}. Since Ni^{4+} is diamagnetic, a decrease of the average chemical shift of the Li signal is expected and can be observed in the experimental spectra. Interestingly at medium SOC ($0.25 \leq x \leq 0.75$), a considerable sharpening of the ^{7}Li signal is observed which is not consistent with the large range of different Li environments expected. This observation can however be explained by an increase in the lithium ion mobility, stimulated by the creation of lithium vacancies and the increasing interlayer spacing, the latter resulting in a reduction in the activation barrier for Li hopping.[14] Fast Li ion hopping between different Li sites can be expected to lead to the observation of an NMR signal at an averaged chemical shift.[31] To substantiate this hypothesis, ^{7}Li MAS NMR spectra at variable temperatures (VT) were recorded for samples with x = 0.1, x = 0.25, and x = 0.5 (Figure 4). An increase in temperature is expected to increase the lithium hopping rate and hence lead to further sharpening of the NMR signals. Indeed, the ^{7}Li signals for x = 0.25 and x = 0.5 sharpen considerably with increasing temperature (Figure 4b,c), whereas the line shape for x = 0.1 remains largely unchanged (Figure 4a). Another indication of fast Li mobility is that the remaining signal after a Hahn echo experiment of one rotor period drops drastically between the x = 0.1 and x = 0.25 samples (see Figure S5b).[31,32] Lithium hopping during the echo period leads to changing resonance frequencies, meaning that refocusing of transverse magnetization becomes inefficient and signal intensity is lost. The line narrowing, the VT spectra and the increased transverse relaxation therefore show that there is fast Li ion mobility in NMC811 which sets in at a delithiation of ~25%. A more quantitative analysis of Li hopping observed by solid-state NMR will be provided in the following section.

Towards the end of charge of NMC811 ($x \geq 0.75$), the ^{7}Li signal broadens and splits into several peaks, indicating that Li hopping slows down substantially. As most of the Ni is now in the diamagnetic 4+ oxidation state, more distinct environments can be observed in the ^{7}Li NMR spectra. The main cause of the resonances shifted to high ppm values are now the $Mn^{4\pm}$–90° interactions, leading to spectral features at ~250 ppm and ~500 ppm which correspond to one and two Mn^{4+} ions in the first coordination shell of lithium (Table 1). In addition to these environments due to less mobile Li ions, a signal due to mobile Li ions can still be identified based on the faster relaxation in Hahn echo experiments with different echo lengths (see Figure S5a). This signal is still very prominent at x = 0.75, but decreases markedly for x > 0.75, indicating the preferred extraction of mobile lithium ions and/or a further decrease of Li mobility, the latter correlated with the collapse of the layer spacing at this SOC.

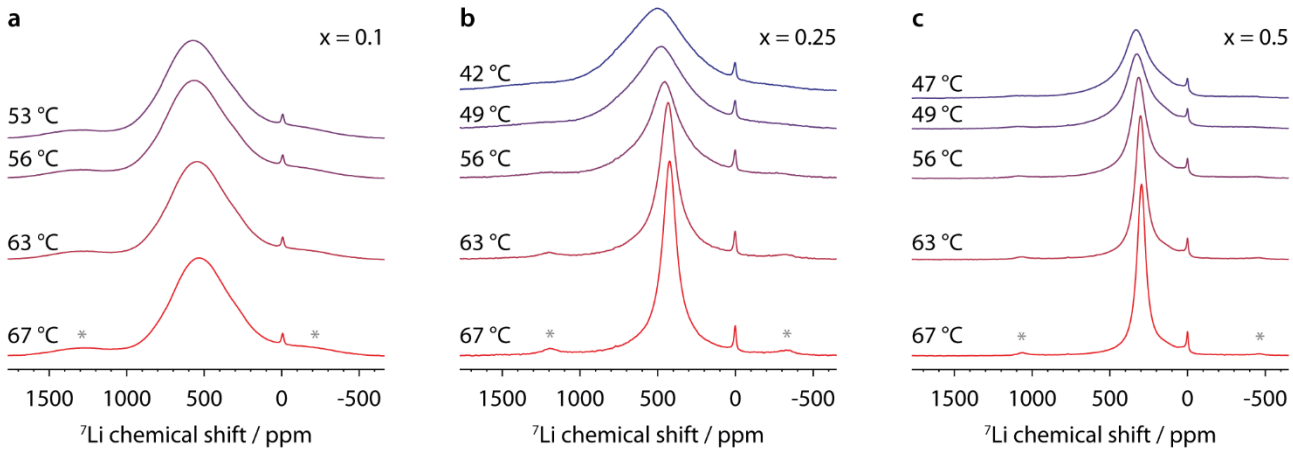

Figure 4. Variable temperature ^{7}Li solid-state NMR spectra of $Li_{1-x}Ni_{0.8}Mn_{0.1}Co_{0.1}O_2$ at three different SOC: (a) $x = 0.1$, (b) $x = 0.25$, (c) $x = 0.5$. Spectra were acquired at 4.7 T under a MAS frequency of 60 kHz, using a Hahn echo pulse sequence. Asterisks in the bottom spectra indicate the positions of spinning sidebands for each series of spectra. Note that the chemical shift in ppm decreases with increasing temperature in all samples, which is typical for signals shifted by Fermi contact interactions. See also Figure S1 for modeling of these spectra.

Calculation of the ^{7}Li NMR spectra. To gain more insights from the NMR data, the expected ^{7}Li NMR spectra were calculated following procedures described earlier.[22,23] In brief, the calculations consider every possible TM environment of a Li ion in this system. For each environment, the corresponding ^{7}Li chemical shift is determined using the hyperfine shifts given in Table 1, and its probability is calculated using the probabilities of encountering Ni, Mn, and Co ions (0.8, 0.1, and 0.1, respectively). A ^{7}Li NMR spectrum is then calculated by summing up the spectra for all environments. This random solution model assumes that TM and Li ions are randomly distributed within their layers. More details on the calculations can be found in the SI.

The calculated spectra for $x = 0.0$ and $x = 0.1$ are shown in Figure 5 and are in good agreement with the respective experimental spectra. Deviations may result from partial ordering of TM ions within their layers, arising from the occurrence of Ni^{2+}–Mn^{4+} pairs or larger clusters of certain TM ions as described for related NMC materials.[30,33]

In order to calculate the spectra in the case of mobile lithium ions for $x > 0.1$, a formula given by Norris was employed.[24] It allows rapid computation of chemical exchange line shapes even when several hundred sites are involved, under the assumption that all Li sites participate in the exchange and that the same hopping rate occurs between all sites.[24] The resulting fits to the experimental spectra of mobile Li ions ($0.25 \leq x \leq 0.65$) are shown in Figure 5, employing a combination of spectra calculated for mobile (blue) and non-mobile (green) Li ions. Excellent agreement between the model and the experimental spectra is obtained. These results show that while a large fraction of Li ions has high mobility, there are also domains with slower Li ion dynamics at a time scale to which these NMR experiments are not sensitive.

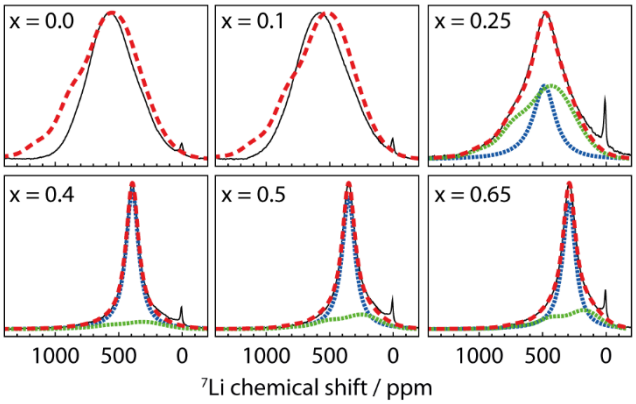

Figure 5. Modeling of ^{7}Li solid-state NMR spectra of $Li_{1-x}Ni_{0.8}Mn_{0.1}Co_{0.1}O_2$. For each SOC, the experimental spectrum is shown (black, identical to Figure 3) together with the calculated spectrum (red). The calculated spectra for $x = 0.0$ and $x = 0.1$ were obtained using the model without Li hopping, whereas the other calculated spectra are the sum (red) of calculations for mobile (blue) and non-mobile (green) Li ions. The peak at ~0 ppm is not included in the model. The calculated spectra for $x \geq 0.75$ and the fraction of mobile Li ions used in the calculations are shown in Figures S4 and S2a, respectively.

The differences in dynamics can be explained by different activation barriers for Li hops which can vary depending on the TM environment and Li/vacancy concentration, as described in the introduction. Accordingly, domains with slower diffusion can be expected to have a high concentration of Li ions and of highly charged TM ions (e.g. Mn^{4+}). The fraction of less mobile Li ions decreases with increasing measurement temperature in the VT experiments (see Figure S2b), demonstrating that the slower diffusion is indeed due to higher activation barriers and not due to particle isolation or disconnection.

For quantifying the Li hopping rates, the linewidths at half height of the calculated ($\nu_{½,calc}$) and experimental ($\nu_{½,exp}$) signals for mobile Li ions were used, the latter determined from deconvoluting the experimental spectra. Since the formula used for calculating the chemical exchange line shapes incorporates the

linewidth of a single Li environment in absence of exchange ($\nu_{½,no\text{-}exch}$),[24] the chosen value influences the hopping rate that is obtained. $\nu_{½,no\text{-}exch}$ is governed by both the ^{7}Li spin-spin relaxation time and inhomogeneous broadening caused by distributions in the local environment. In our case, it cannot be determined experimentally because the signals from different Li environments overlap. Therefore, three different values were employed for computing $\nu_{½,calc}$ and consequently the hopping rates. The results for different SOC are plotted in Figure 6. The smallest value used ($\nu_{½,no\text{-}exch}$ = 100 Hz, triangles) is undoubtedly smaller than the experimental value and returns the lowest hopping rate. The maximum value for $\nu_{½,no\text{-}exch}$ (2000 Hz, circles) was chosen based on the consideration that the sharpest line obtained experimentally (for x = 0.5 at high temperature) can only be modelled if $\nu_{½,no\text{-}exch} \leq 2500$ Hz. While exact hopping rates are difficult to extract from the NMR data, clear trends of lithium mobility can be obtained as illustrated in Figure 6. Li ion hopping sets in between x = 0.1 and x = 0.25 and reaches a maximum at x = 0.4 with a hopping rate of at least 58 kHz. It then remains at this high level until x = 0.65, slightly decreasing on further delithiation. A clear drop in lithium mobility is seen for $x \geq 0.75$.

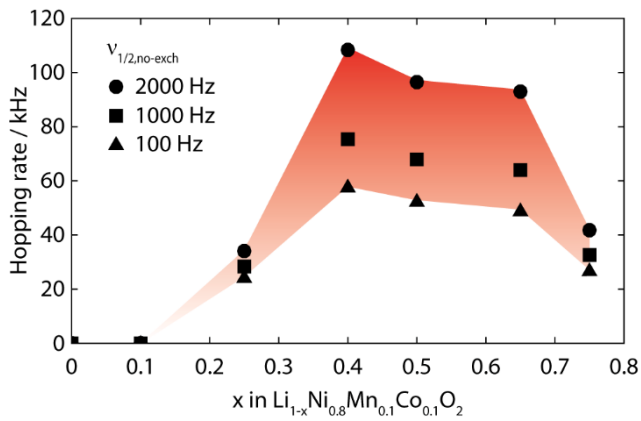

Figure 6. Li ion hopping rates at different SOC calculated from line widths of ^{7}Li NMR signals. Different $\nu_{½,no\text{-}exch}$ values were used for the computation of spectra, with the triangles representing the minimum Li ion hopping rates. Red shading has been added for illustrational purposes.

At this high SOC ($x \geq 0.75$), a straightforward fitting of the experimental spectra with the model described above is no longer possible (see Figure S4), and in particular the relative peak intensities are not well-reproduced. This can be related to lithium/vacancy ordering at high SOC where signals originating from Li ions in their preferred TM environments will dominate the NMR spectrum. For example, purely diamagnetic environments as well as Mn^{4+}–180° interactions do not appear to be favored because no substantial peak intensity at negative chemical shifts can be observed. On the other hand, Mn^{4+}–90° interactions are favorable which is shown by their relatively higher peak intensities, meaning that local environments containing these environments are observed in higher concentrations than predicted by the random solution model. Modelling and understanding effects from TM ordering and Li/vacancy ordering on the ^{7}Li NMR spectra is beyond the scope of this report and will be the subject of further research.

GITT measurements. GITT was employed as an additional method to probe the change in lithium dynamics as a function of SOC. For a GITT experiment, the cell voltage is monitored as short pulses at a constant current are applied, interrupted by long rest periods during which no current passes through the cell.[16] A typical voltage and current profile of the cell during one pulse and rest period is shown in Figure S11. The OCV profile of the NMC 811 material during the GITT experiment is presented in Figure 7a and the extracted results on lithium mobility are summarized in Figure 7b. Due to the difficulty in accurately obtaining the values of the active surface area (S) and the molar volume (V_m) of the NMC material, we use the proxy of $D_s S^{-2} V_m^{-2}$, denoted as Li mobility in Figure 7b, for the Li^+ diffusivity to compare the relative Li dynamics as a function of SOC (see also Materials and Methods).

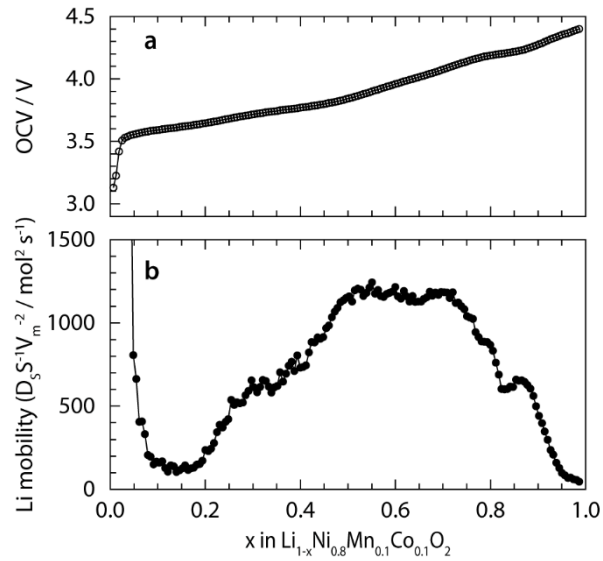

Figure 7. OCV curve (a) and Li mobility (b) obtained from GITT applied to NMC811/Li half-cells. The first points in (b) (x < 0.1) overestimate the Li mobility because the cell potential was not fully relaxed when the next current pulse was applied.

The OCV profile matches the voltage profile under conventional galvanostatic cycling conditions (Figure 1a). For instance, the flatter voltage region at ~4.2 V is observed in both results. This confirms that these electrochemical signatures are associated with the intrinsic properties at equilibrated states of the material, rather than artefacts induced by kinetics or mass-transport which are likely to occur in galvanostatic cycling experiments. These signatures correlate with the evolution of the Li mobility extracted from the GITT on the first charge (Figure 7b). Li mobility gradually increases from 20% SOC and reaches a maximum at ~50% SOC. Of note, the maximum Li mobility is one order-of-magnitude higher than that at 20% SOC. The Li diffusion remains at this very high level as the charge continues, until approximately 70% SOC, from when it starts dropping drastically. This overall trend in the evolution of Li mobility agrees very well with the findings from NMR experiments.

DISCUSSION

Structural and dynamic changes upon delithiation of NMC811. The set of experimental data presented above shows

that the delithiation of NMC811 cathodes can be divided into four regions as highlighted in Figure 1, which can be related to changes in the structure and Li dynamics of the material.

The beginning of charge (0–50 mAh g^{-1}, $0 \leq x \leq 0.18$) is marked by broad NMR spectra, indicating low Li mobility. Li ion hopping then increases drastically in the second part of region I (50–125 mAh g^{-1}, $0.18 \leq x \leq 0.45$) which is defined by a broad and intense peak in the dQ/dV plot. The increasing Li mobility is apparent in both the NMR spectra and the GITT data and is stimulated by the creation of Li (di)vacancies as well as the substantial increase in Li layer spacing which is shown by the XRD data. The former increases the number of carriers while the latter lowers the activation barrier for Li hops which can also be seen from the VT NMR experiments (Figure S3). The NMR data additionally shows that Li hopping rates are not uniform throughout the sample, and that domains with slower Li dynamics exist, especially when Li mobility starts to increase ($x = 0.25$). The maximum Li hopping rate is observed at $x = 0.4$ in the NMR data and at $x \sim 0.5$ in the GITT data.

Region II (125–195 mAh g^{-1}, $0.45 \leq x \leq 0.70$) is characterized by a very broad peak in the dQ/dV plot, corresponding to a steeper voltage increase with continuing delithiation. The lithium mobility remains high in this regime, but does not increase further. This can be rationalized by the less steep increase of the *c* lattice parameter and the creation of more highly charged TM ions which hinder faster diffusion.

A drastic change occurs in region III (195–220 mAh g^{-1}, $0.70 \leq x \leq 0.78$) which is marked by a clear peak in the dQ/dV plot. While this peak has been hypothesized to indicate a detrimental two-phase O3→O1 transition as it is observed in $LiNiO_2$, no signature of such a transition is observed in the *operando* XRD data, which is in accordance with other reports in literature.[4,11] Region III is nevertheless marked by a strong decrease of the *c* lattice parameter. This collapse of the interlayer spacing is accompanied by decreasing Li mobility, indicated again both in the NMR and in the GITT data.

Towards the end of charge (region IV, >220 mAh g^{-1}, $x > 0.78$), the collapse of the *c* lattice parameter becomes even more drastic and it drops below its initial value, accompanied by a steep decrease of the unit cell volume. This further slows down Li diffusion, and results in Li/vacancy ordering which can be seen from the NMR data where fitting with a simple random solution model is no longer possible (Figure S4). The NMR spectra suggest that Mn^{4+}–90° interactions are preferred by Li ions whereas purely diamagnetic environments (i.e., Li nearby Ni^{4+} ions) as well as Mn^{4+}–180° interactions appear less favorable. The structural changes at high SOC as well as the slow Li diffusion hinder the further extraction of Li ions. Accordingly, no significant additional capacity can be achieved even when charging up to 4.8 V (see Figure S6).

Reexamining the NMR spectra in the literature, where line narrowing and/or faster transverse relaxation are observed upon electrochemical delithiation, it is clear that similar Li mobility is present to a degree in many NMCs and related layered materials.[31,34–36] For example, a sharper NMR resonance emerges for 20% Li removal in NMC111, coexisting with a broader resonance.[34] Based on the results presented here, this likely also originates from a subset of more mobile Li ions.

CONCLUSIONS

Operando XRD, *ex situ* ^{7}Li solid-state MAS NMR, and GITT have been used to correlate changes in structure and lithium dynamics upon electrochemical cycling of NMC811. An increase in the interlayer spacing up to ~70% SOC together with the creation of Li vacancies is accompanied by a strong increase in Li ion mobility. Fast Li ion hopping sets in at ~20% SOC and reaches a maximum between 40% and 50% SOC. Above 70% SOC, the overall layer spacing and with it the unit cell volume collapses rapidly, with the Li layer spacing collapsing slightly later from ~75% SOC. This leads to decreased Li mobility as well as Li/vacancy ordering, and makes it harder to extract more Li ions, preventing access to capacity associated with the remaining lithium.

The *operando* synchrotron XRD data clearly show that no two-phase O3→O1 transition occurs at high SOC of NMC811, meaning that this cannot be a major cause of degradation. However, pronounced changes of the *c* lattice parameter are still observed, most notably its collapse above ~70% SOC. These anisotropic lattice expansions are expected to lead to strain within particles which can eventually cause particle cracking after prolonged cycling. Such effects can in principle be mitigated by cycling to lower cutoff potentials (~4.2 V vs Li^+/Li), avoiding strong overall layer contractions. Li mobility would also remain high in this cycling regime, allowing faster charging rates to be used without serious detrimental effects due to, for example, heat evolution or heterogeneity in lithiation across the electrode. However, the choice of this comparably low cutoff voltage also reduces the available capacity, removing one of the advantages of using NMC811. Future studies will focus on the role of cation doping (e.g., Mg in the Li layers[37]) and Ni defects in the Li layers on Li mobilities and *c*-parameter changes.

^{7}Li solid-state NMR has been shown to be a useful tool for examining Li mobility, even in challenging paramagnetic materials like NMC811. Li hopping rates can be estimated and distributions of correlation times for Li transport can be identified and associated with specific local environments, which is a phenomenon that is not readily extracted from GITT. This extended characterization of Li mobility will be important for understanding the rate performance and degradation of LIBs in more detail.

ASSOCIATED CONTENT

Supporting Information. ^{7}Li solid-state NMR: details on the calculation of spectra, calculated VT NMR spectra, fractions of mobile Li ions, Arrhenius plot for VT NMR data, calculated spectra at high SOC, spin-spin relaxation in NMC811 samples; structure refinement from X-ray and neutron diffraction data; *operando* XRD: evolution of unit cell parameters for three different samples, enlarged view of XRD patterns, evolution of layer spacing; neutron diffraction pattern of NMC811; typical voltage and current profile during a GITT experiment. This material is available free of charge via the Internet at http://pubs.acs.org.

AUTHOR INFORMATION

Corresponding Author

*E-mail: cpg27@cam.ac.uk

Author Contributions

The manuscript was written through contributions of all authors. All authors have given approval to the final version of the manuscript.

ACKNOWLEDGMENT

This work was funded by the ISCF Faraday Challenge Fast Start project on "Degradation of Battery Materials" made available through grant EP/S003053/1. P.J.R. acknowledges the NorthEast Center for Chemical Energy Storage (NECCES), an Energy Frontier Research Center funded by the U.S. Department of Energy, Office of Science, Office of Basic Energy Sciences, under Award DE-SC0012583. K.J.G. acknowledges support from The Winston Churchill Foundation of the United States, a Herchel Smith Scholarship and a Science and Technology Facilities Council (STFC) Futures Early Career Award. K.J.G. and C.P.G. thank the EPSRC for a LIBATT grant (EP/M009521/1). This work is based upon experiments performed at the SPODI instrument operated by KIT and TUM at the Heinz Maier-Leibnitz Zentrum (MLZ), Garching, Germany. K.J.G. gratefully acknowledges the financial support provided by TUM to perform the neutron scattering measurements. This research also used resources of the Advanced Photon Source, a U.S. Department of Energy (DOE) Office of Science User Facility operated for the DOE Office of Science by Argonne National Laboratory under Contract No. DE-AC02-06CH11357. K.J.G. is grateful for experimental support from beamline scientists Anatoliy Senyshyn, Kamila Wiaderek, and Wenqian Xu.

REFERENCES

(1) Blomgren, G. E. The Development and Future of Lithium Ion Batteries. *J. Electrochem. Soc.* **2017**, *164* (1), A5019–A5025.

(2) Noh, H.-J.; Youn, S.; Yoon, C. S.; Sun, Y.-K. Comparison of the Structural and Electrochemical Properties of Layered $Li[Ni_xCo_yMn_z]O_2$ (x = 1/3, 0.5, 0.6, 0.7, 0.8 and 0.85) Cathode Material for Lithium-Ion Batteries. *J. Power Sources* **2013**, *233*, 121–130.

(3) Manthiram, A.; Song, B.; Li, W. A Perspective on Nickel-Rich Layered Oxide Cathodes for Lithium-Ion Batteries. *Energy Storage Mater.* **2017**, *6*, 125–139.

(4) Li, J.; Downie, L. E.; Ma, L.; Qiu, W.; Dahn, J. R. Study of the Failure Mechanisms of $LiNi_{0.8}Mn_{0.1}Co_{0.1}O_2$ Cathode Material for Lithium Ion Batteries. *J. Electrochem. Soc.* **2015**, *162* (7), A1401–A1408.

(5) Jung, R.; Metzger, M.; Maglia, F.; Stinner, C.; Gasteiger, H. A. Oxygen Release and Its Effect on the Cycling Stability of $LiNi_xMn_yCo_zO_2$ (NMC) Cathode Materials for Li-Ion Batteries. *J. Electrochem. Soc.* **2017**, *164* (7), A1361–A1377.

(6) Jung, R.; Morasch, R.; Karayaylali, P.; Phillips, K.; Maglia, F.; Stinner, C.; Shao-Horn, Y.; Gasteiger, H. A. Effect of Ambient Storage on the Degradation of Ni-Rich Positive Electrode Materials (NMC811) for Li-Ion Batteries. *J. Electrochem. Soc.* **2018**, *165* (2), A132–A141.

(7) Li, J.; Camardese, J.; Glazier, S.; Dahn, J. R. Structural and Electrochemical Study of the Li–Mn–Ni Oxide System within the Layered Single Phase Region. *Chem. Mater.* **2014**, *26* (24), 7059–7066.

(8) Li, W.; Reimers, J.; Dahn, J. In Situ X-Ray Diffraction and Electrochemical Studies of $Li_{1-x}NiO_2$. *Solid State Ionics* **1993**, *67* (1–2), 123–130.

(9) Li, H.; Zhang, N.; Li, J.; Dahn, J. R. Updating the Structure and Electrochemistry of Li_xNiO_2 for $0 \leq x \leq 1$. *J. Electrochem. Soc.* **2018**, *165* (13), A2985–A2993.

(10) Delmas, C.; Fouassier, C.; Hagenmuller, P. Structural Classification and Properties of the Layered Oxides. *Phys. B+C* **1980**, *99* (1–4), 81–85.

(11) Ryu, H.-H.; Park, K.-J.; Yoon, C. S.; Sun, Y.-K. Capacity Fading of Ni-Rich $Li[Ni_xCo_yMn_{1-x-y}]O_2$ ($0.6 \leq x \leq 0.95$) Cathodes for High-Energy-Density Lithium-Ion Batteries: Bulk or Surface Degradation? *Chem. Mater.* **2018**, *30* (3), 1155–1163.

(12) Radin, M. D.; Hy, S.; Sina, M.; Fang, C.; Liu, H.; Vinckeviciute, J.; Zhang, M.; Whittingham, M. S.; Meng, Y. S.; Van der Ven, A. Narrowing the Gap between Theoretical and Practical Capacities in Li-Ion Layered Oxide Cathode Materials. *Adv. Energy Mater.* **2017**, *7* (20), 1602888.

(13) Van der Ven, A.; Ceder, G. Lithium Diffusion Mechanisms in Layered Intercalation Compounds. *J. Power Sources* **2001**, *97–98*, 529–531.

(14) Kang, K.; Ceder, G. Factors That Affect Li Mobility in Layered Lithium Transition Metal Oxides. *Phys. Rev. B* **2006**, *74* (9), 094105.

(15) Van der Ven, A.; Bhattacharya, J.; Belak, A. A. Understanding Li Diffusion in Li-Intercalation Compounds. *Acc. Chem. Res.* **2013**, *46* (5), 1216–1225.

(16) Weppner, W. Determination of the Kinetic Parameters of Mixed-Conducting Electrodes and Application to the System Li_3Sb. *J. Electrochem. Soc.* **1977**, *124* (10), 1569.

(17) Verma, A.; Smith, K.; Santhanagopalan, S.; Abraham, D.; Yao, K. P.; Mukherjee, P. P. Galvanostatic Intermittent Titration and Performance Based Analysis of $LiNi_{0.5}Co_{0.2}Mn_{0.3}O_2$ Cathode. *J. Electrochem. Soc.* **2017**, *164* (13), A3380–A3392.

(18) Hoelzel, M.; Senyshyn, A.; Juenke, N.; Boysen, H.; Schmahl, W.; Fuess, H. High-Resolution Neutron Powder Diffractometer SPODI at Research Reactor FRM II. *Nucl. Instruments Methods Phys. Res. Sect. A Accel. Spectrometers, Detect. Assoc. Equip.* **2012**, *667*, 32–37.

(19) Borkiewicz, O. J.; Shyam, B.; Wiaderek, K. M.; Kurtz, C.; Chupas, P. J.; Chapman, K. W. The AMPIX Electrochemical Cell: A Versatile Apparatus for in Situ X-Ray Scattering and Spectroscopic Measurements. *J. Appl. Crystallogr.* **2012**, *45* (6), 1261–1269.

(20) Hung, I.; Zhou, L.; Pourpoint, F.; Grey, C. P.; Gan, Z. Isotropic High Field NMR Spectra of Li-Ion Battery Materials with Anisotropy >1 MHz. *J. Am. Chem. Soc.* **2012**, *134* (4), 1898–1901.

(21) Bielecki, A.; Burum, D. P. Temperature Dependence of ^{207}Pb MAS Spectra of Solid Lead Nitrate. An Accurate, Sensitive Thermometer for Variable-Temperature MAS. *J. Magn. Reson. Ser. A* **1995**, *116* (2), 215–220.

(22) Pan, C.; Lee, Y. J.; Ammundsen, B.; Grey, C. P. ^6Li MAS NMR Studies of the Local Structure and Electrochemical Properties of Cr-Doped Lithium Manganese and Lithium Cobalt Oxide Cathode Materials for Lithium-Ion Batteries. *Chem. Mater.* **2002**, *14* (5), 2289–2299.

(23) Trease, N. M.; Seymour, I. D.; Radin, M. D.; Liu, H.; Liu, H.; Hy, S.; Chernova, N.; Parikh, P.; Devaraj, A.; Wiaderek, K. M.; et al. Identifying the Distribution of Al^{3+} in $LiNi_{0.8}Co_{0.15}Al_{0.05}O_2$. *Chem. Mater.* **2016**, *28* (22), 8170–8180.

(24) Norris, J. R. Rapid Computation of Magnetic Resonance Line Shapes for Exchange among Many Sites. *Chem. Phys. Lett.* **1967**, *1* (8), 333–334.

(25) Croguennec, L.; Pouillerie, C.; Delmas, C. NiO_2 Obtained by Electrochemical Lithium Deintercalation from Lithium Nickelate: Structural Modifications. *J. Electrochem. Soc.* **2000**, *147* (4), 1314.

(26) Grenier, A.; Liu, H.; Wiaderek, K. M.; Lebens-Higgins, Z. W.; Borkiewicz, O. J.; Piper, L. F. J.; Chupas, P. J.; Chapman, K. W. Reaction Heterogeneity in $LiNi_{0.8}Co_{0.15}Al_{0.05}O_2$ Induced by Surface Layer. *Chem. Mater.* **2017**, *29* (17), 7345–7352.

(27) Grey, C. P.; Dupré, N. NMR Studies of Cathode Materials for Lithium-Ion Rechargeable Batteries. *Chem. Rev.* **2004**, *104* (10), 4493–4512.

(28) Carlier, D.; Ménétrier, M.; Grey, C. P.; Delmas, C.; Ceder, G. Understanding the NMR Shifts in Paramagnetic Transition Metal Oxides Using Density Functional Theory Calculations. *Phys. Rev. B* **2003**, *67* (17), 174103.

(29) Ammundsen, B.; Paulsen, J. Novel Lithium-Ion Cathode Materials Based on Layered Manganese Oxides. *Adv. Mater.* **2001**, *13* (12–13), 943–956.

(30) Zeng, D.; Cabana, J.; Bréger, J.; Yoon, W.-S.; Grey, C. P. Cation Ordering in $Li[Ni_xMn_xCo_{(1-2x)}]O_2$-Layered Cathode Materials: A Nuclear Magnetic Resonance (NMR), Pair Distribution Function, X-Ray Absorption Spectroscopy, and Electrochemical Study. *Chem. Mater.* **2007**, *19* (25), 6277–6289.

(31) Carlier, D.; Ménétrier, M.; Delmas, C. ^{7}Li MAS NMR Study of Electrochemically Deintercalated $Li_xNi_{0.30}Co_{0.70}O_2$ Phases: Evidence of Electronic and Ionic Mobility, and Redox Processes. *J. Mater. Chem.* **2001**, *11* (2), 594–603.

(32) Zhou, L.; Leskes, M.; Liu, T.; Grey, C. P. Probing Dynamic Processes in Lithium-Ion Batteries by In Situ NMR Spectroscopy: Application to $Li_{1.08}Mn_{1.92}O_4$ Electrodes. *Angew. Chemie Int. Ed.* **2015**, *54* (49), 14782–14786.

(33) Harris, K. J.; Foster, J. M.; Tessaro, M. Z.; Jiang, M.; Yang, X.; Wu, Y.; Protas, B.; Goward, G. R. Structure Solution of Metal-Oxide Li Battery Cathodes from Simulated Annealing and Lithium NMR Spectroscopy. *Chem. Mater.* **2017**, *29* (13), 5550–5557.

(34) Yoon, W.-S.; Grey, C. P.; Balasubramanian, M.; Yang, X.-Q.; Fischer, D. A.; McBreen, J. Combined NMR and XAS Study on Local Environments and Electronic Structures of Electrochemically Li-Ion Deintercalated $Li_{1-x}Co_{1/3}Ni_{1/3}Mn_{1/3}O_2$ Electrode System. *Electrochem. Solid-State Lett.* **2004**, *7* (3), A53.

(35) Chazel, C.; Ménétrier, M.; Croguennec, L.; Delmas, C. Coupled Ion/Electron Hopping in Li_xNiO_2: A ^{7}Li NMR Study. *Inorg. Chem.* **2006**, *45* (3), 1184–1191.

(36) Zeng, D.; Cabana, J.; Yoon, W.-S.; Grey, C. P. Investigation of the Structural Changes in $Li[Ni_yMn_yCo_{(1-2y)}]O_2$ (y = 0.05) upon Electrochemical Lithium Deintercalation. *Chem. Mater.* **2010**, *22* (3), 1209–1219.

(37) Xie, Q.; Li, W.; Manthiram, A. A Mg-Doped High-Nickel Layered Oxide Cathode Enabling Safer, High-Energy-Density Li-Ion Batteries. *Chem. Mater.* **2019**, *31* (3), 938–946.
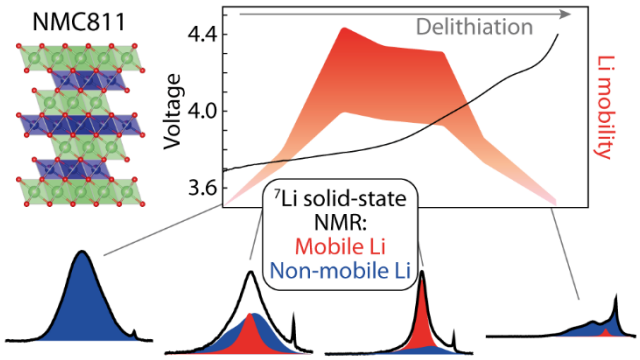
Table of Contents artwork: